https://doi.org/10.1016/j.apenergy.2016.06.121

Parameter sensitivity analysis and configuration optimization of indirect evaporative cooler (IEC) considering condensation

Yi Chen[a], Hongxing Yang[a], Yimo Luo[b,*]

[a]*Renewable Energy Research Group (RERG), Department of Building Services Engineering, The Hong Kong Polytechnic University, Hong Kong*

[b]*Faculty of Science and Technology, Technological and Higher Education of Institute of Hong Kong, Hong Kong*

Abstract

The indirect evaporative cooler (IEC) is a low-carbon device which cools the air with water evaporation. Its performances in dry regions have been investigated intensively. However, its application in hot and humid regions, where the IEC is used as a pre-cooling device in an air-conditioning system, is still at developing stage. The exhausted air from air-conditioned space is humidified and used as secondary air to pre-cool the fresh air. As the dew point temperature of the fresh air is high, condensation may occur in the dry channels. However, the parameter sensitivity analysis of IEC with condensation is lacking. Besides, the optimized IEC configuration may be different from that of dry regions because of distinguished air handling process. So the sensitivity analysis among seven parameters by orthogonal test was conducted based on the experimental-validated IEC model emphasizing on condensation condition. The optimization was then conducted to the most influential and engineering controllable parameters. The results indicate the channel gap and cooler height are the key influential factors on IEC thermal performance. The optimized channel gap is 2~3mm and 3~4mm under condensation and non-condensation state, respectively. The optimized NTU_p is 4~7 and 3~5, respectively.

* Corresponding author. E-mail address: yimo.luo@vtc.edu.hk
This paper was significantly revised based on the short version, which was presented at the CUE2015- Applied Energy Symposium and Summit 2015: low carbon cities and urban energy systems in Nov 2016, Fuzhou, China.

Keywords: indirect evaporative cooler, condensation, orthogonal test, sensitivity analysis, optimization

1. Introduction

Indirect evaporative cooler (IEC) is an energy efficient and environmental friendly cooling device which uses water evaporation to produce cooling air [1, 2]. The IEC has been regarded as a promising energy-saving technology in the near future for its high efficient, low energy consumption, pollution-free and easy maintenance features [3~5]. The most commonly used plate-type IEC consists of alternative wet and dry channels which are separated by thin plates. In the wet channels, the spraying water drops form a thin water film on the plate surface and consistently evaporates into the main stream of secondary air. The primary air in the adjacent dry channels is sensibly cooled by the low temperature wall without change in moisture content [6]. The schematic diagram of a typical plate type counter flow IEC is shown in Fig.1. The channel gap is an important geometric parameter which refers to the gap between adjacent plates in IEC.

The air with lower humidity provides larger evaporation driving force, so larger cooling capacity can be achieved when IEC applied in hot and dry regions. The cooled primary air is supplied to the interior directly in these regions [7~9]. But in hot and humid regions, its application is restricted because the supplied primary air temperature is limited to the high wet-bulb temperature of ambient air. However, in recent years, a new hybrid air-conditioning system consisted of IEC and mechanical cooling is proposed for IEC application in hot and humid regions [10~15]. The IEC, installed before an AHU or cooling coil, is used to pre-cool the fresh air for energy conservation. The exhausted air with lower temperature and humidity from air-

conditioned space is used as secondary air for enhancing the evaporation process. Unlike the normal cases in which the IEC operates for only sensible cooling in dry regions, condensation from high humidity primary air may occurs when IEC applied in humid regions, resulting in not only sensible cooling but also dehumidification effect. However, it is found that relevant study on IEC with condensation is still at developing stage [16].

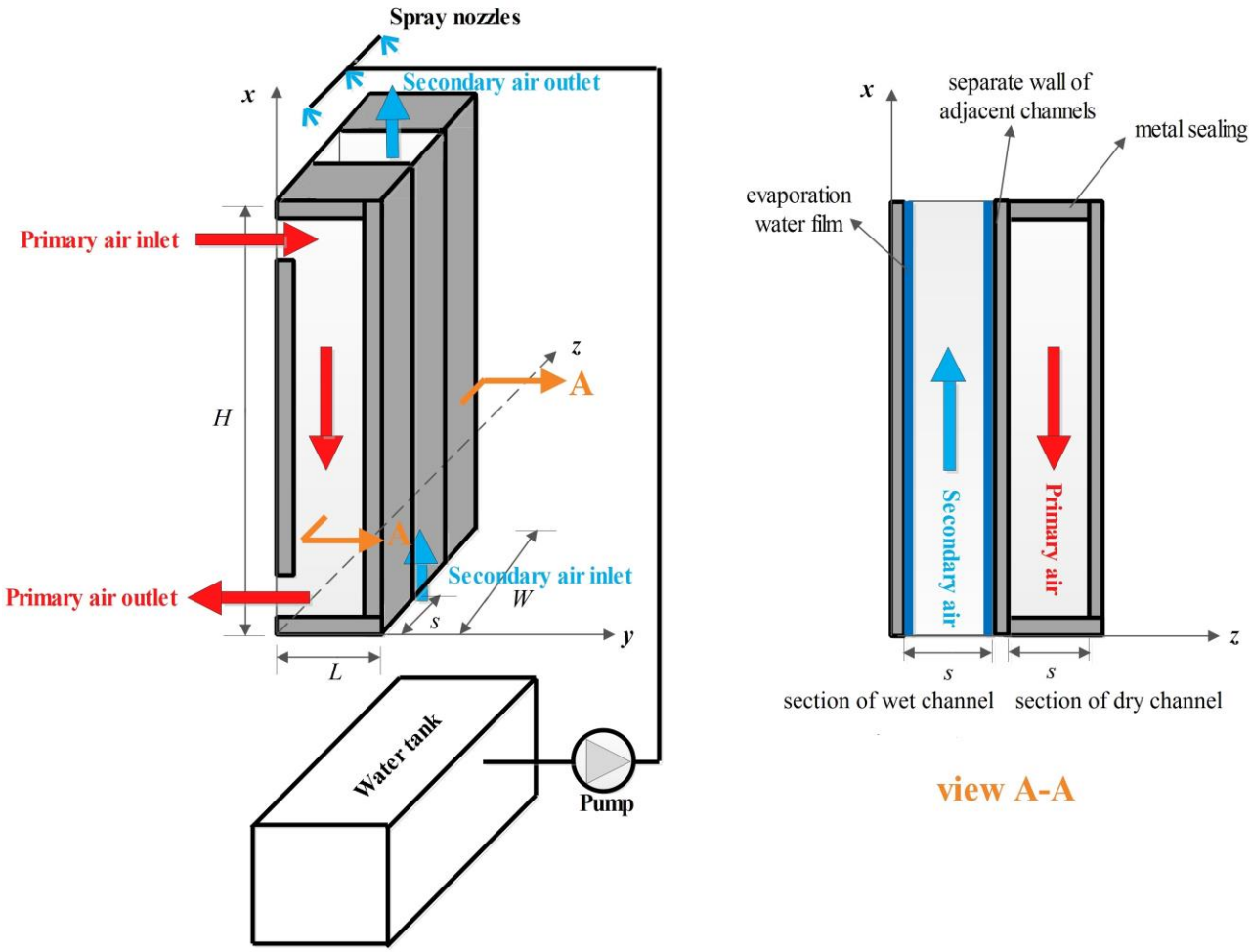

Fig.1 Schematic diagram of plate type counter flow IEC

For high efficient cooling system, the parameter study, sensitivity analysis and configuration optimization are crucial because they could provide valuable guidance for favorable operating conditions and system design. A lot of such studies have been conducted to IEC under its non-

condensation state. The models of IEC including traditional IEC, RIEC, M-cycle IEC (a dew-point IEC proposed by Dr. Maisotsenko [17]) and other dew-point IEC [18] were established and solved numerically or analytically to investigate the influence of inlet air conditions (temperature, humidity and velocity) and unit geometry on its performances [19~25]. A sensitivity analysis was performed by Bolotin et al. [26] based on ε-NTU method to determine the preferable operating conditions for the cross-type typical IEC and RIEC. Kim et al. [27] conducted a comprehensive sensitivity study by 2^k-factorical experiment design approach. The influence ranking of seven parameters was obtained and a practical thermal performance correlation was derived by linear regression. The optimization of IEC mainly includes the optimization of NTU_p, geometry size and air flow ratio. A global optimization method based on the entransy theory was proposed to be applied on the evaporative cooling systems by Yuan and Chen [28]. The optimal NTU_p to achieve maximum efficiency of IEC was discussed among three commercial prototypes [29] as well as a cross-flow dew-point IEC [30]. Pandelidis and Anisimov [31] conducted an optimization study on the hole arrangement and size of the secondary and primary part in the dry channels of M-cycle IEC. Anisimov et al. [32] proposed a novel combined parallel and counter flow RIEC and optimized NTU_p and air flow ratio accordingly. Goldsworthy and White [33] optimized the regeneration temperature and supply/regeneration flow ratio of a desiccant IEC cooling system. In sum, the parameter study, sensitivity analysis and configuration optimization of IEC operates under non-condensation state had been well investigated.

However, the research on IEC with condensation is very limited. Cui et al. [34] established a numerical model of IEC with condensation and validated the model by published data. Yang et al. [35] developed an analytical model of IEC with condensation based on ε-NTU method. But the

intensive parameter study, sensitivity analysis and optimization were not presented. So a numerical model of IEC considering condensation was established by us using a different method and intensive parameter study was conducted in our previous paper [36]. It can be deduced that the optimized IEC configuration under condensation state may differ from that of non-condensation state because of distinguished heat and mass transfer process. So a follow-up research is conducted in this paper based on the previous publication. It aims to fill the research gap of parameter sensitivity analysis and configuration optimization of IEC under condensation state.

The detail research flow chart is shown in Fig.2. Firstly, an IEC model considering condensation was introduced and validated by the experimental data. Then, seven parameters (t_p, RH_p, t_s, RH_s, u_p/u_s, s, H) were selected for parameter sensitivity analysis. The orthogonal test was designed and simulations results were analyzed. At last, the most influential and engineering controllable parameters were optimized.

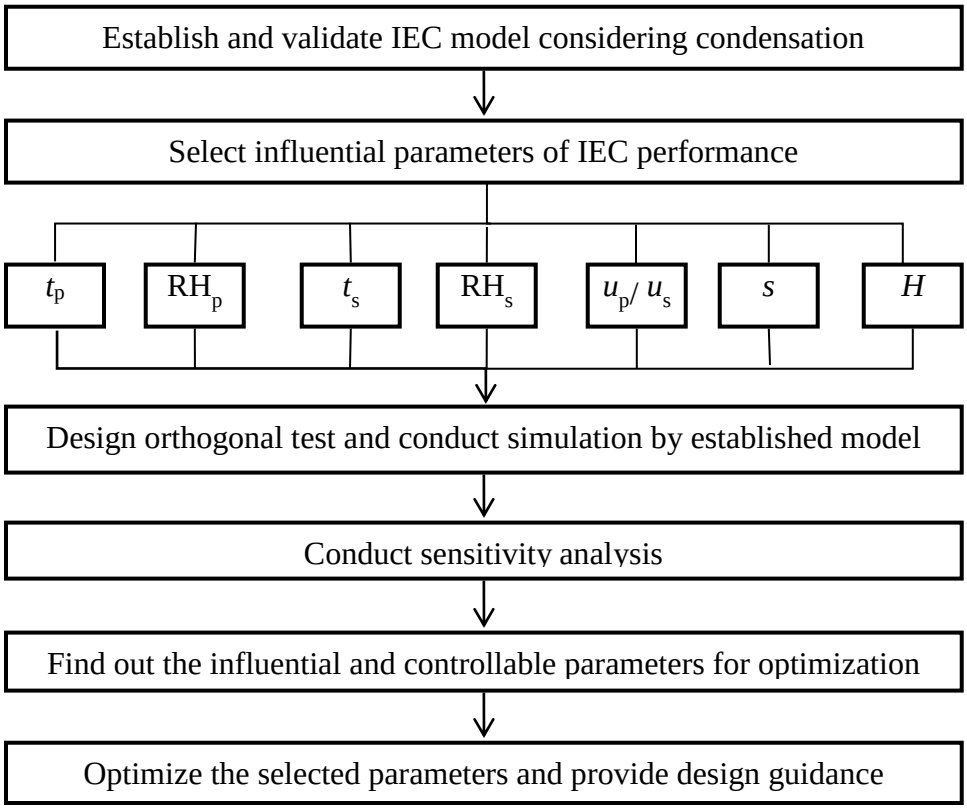

Fig.2 Research flow chart for parameter sensitivity analysis and optimization

Nomenclatures

A	heat transfer area, m^2	h	heat transfer coefficient, $W/m^2 \cdot ℃$
H	cooler height, m	h_m	mass transfer coefficient, $kg/m^2 \cdot s$
L	cooler length, m	h_{fg}	latent heat of vaporization of water, J/kg
P	pressure, pa	i	enthalpy of air, $J/kg \cdot ℃$
Pr	Prandtl number	m	mass flow rate, kg/s
NTU	number of heat transfer unit	n	number of channels
c_{pa}	specific heat of air, $J/kg \cdot ℃$	s	channel gap, m
c_{pw}	specific heat of water, $J/kg \cdot ℃$	t	Celsius temperature, ℃
d_e	hydraulic diameter of channel, m	u	air velocity, m/s

Greek symbols			
ω	moisture content of air, kg/kg	μ	dynamic viscosity, Pa·s
σ	wettability	υ	kinematic viscosity, m^2/s
η	efficiency	λ	thermal conductivity, W/m·℃
ε	enlargement coefficient		
Subscripts			
c	condensation	*ew*	evaporation water
e	evaporation	*in*	air inlet
p	primary/fresh air	*out*	air outlet
s	secondary/exhaust air	*wb*	wet-bulb
w	wall	*lat*	latent heat transfer
cw	condensate water		
Abbreviation			
RH	relative humidity	RIEC	regenerative indirect evaporative cooler
IEC	indirect evaporative cooler	COP	coefficient of performance

2. Modeling and validation

2.1 Modeling of IEC considering condensation

2.1.1 Thermal performance

According to different inlet air conditions, two possible operation states of IEC can be identified, which are non-condensation and condensation, as shown in Fig.3. Non-condensation state occurs when the inlet primary air is dry and the dew point temperature is always lower than the plate surface temperature. Condensation state occurs when the inlet primary air is very humid so that

the dew point temperature is higher than the plate surface temperature somewhere. The latter state may take place when the IEC is applied in hot and humid regions for pre-cooling in an air-conditioning system, in which the primary air humidity is high while the wet-bulb temperature of secondary air from air-conditioned space is relatively low.

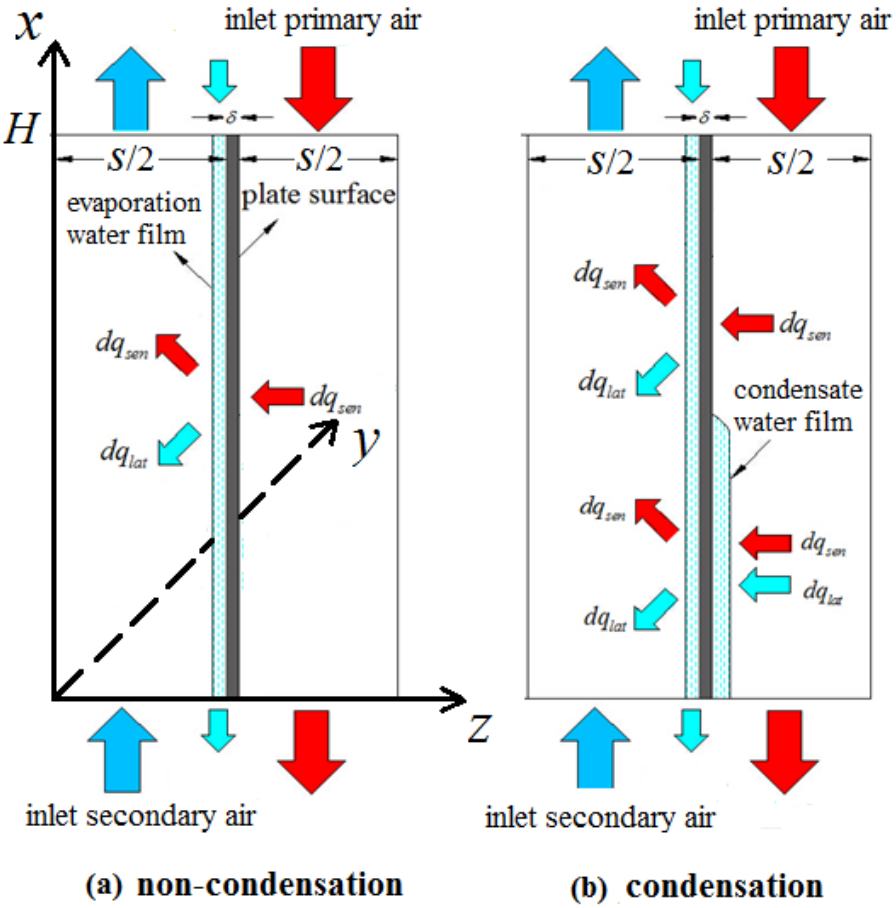

Fig.3 Schematic diagram of two possible operation states of IEC

The IEC model is established based on the thermal and moisture balances in the two channels and the whole system. The model is introduced briefly as follows. The details can be referred to the previous published paper [36]. Several assumptions are made before the model developed, including: 1) no heat loss to the surroundings; 2) thermal resistances of water film and wall are negligible; 3) heat and mass are transferred vertically across the separated plate; 4) water film is

continuously replenished at the same temperature; 5) Lewis number is unity in both evaporation and condensation surface; 6) flow pattern is counter flow.

The governing equations can be written in standard ordinary differential equations as Eq.(1) to (8), including the heat balances (Eq.(1), (3)), moisture balances (Eq.(2), (4)), water mass balances (Eq.(5), (6)) and the corresponding wall temperature under the non-condensation and condensation state (Eq.(7), (8)). Then, the differential term is discretized into algebraic form by finite difference method (FDM) and numerical simulation results at each discrete node can be obtained by solving a set of algebraic equations simultaneously. As there are two possible operation states of IEC, judgement on whether condensation takes place should be made at each calculation step on each discrete node by comparing ω_p and ω_{t_w}

$$\frac{dt_s}{dx^*} = NTU_s(t_w - t_s) \quad (1)$$

$$\frac{d\omega_s}{dx^*} = \sigma NTU_{ms}(\omega_{t_w} - \omega_s) \quad (2)$$

$$\frac{dt_p}{dx^*} = NTU_p(t_p - t_w) \quad (3)$$

$$\frac{d\omega_p}{dx^*} = NTU_{mp}(\omega_p - \omega_{t_w}) \text{ (if } \omega_p > \omega_{t_w}) \quad (4)$$

$$\frac{dm_{ew}}{dx^*} = \sigma NTU_e(\omega_{t_w} - \omega_s) \quad (5)$$

$$\frac{dm_{cw}}{dx^*} = -NTU_c(\omega_p - \omega_{t_w}) \text{ (if } \omega_p > \omega_{t_w}) \quad (6)$$

$$t_w = c_1 t_p + c_2 \omega_s + c_3 t_s + c_4 (if\ \omega_p > \omega_{t_w}) \quad (7)$$

$$t_w = c_5 t_p + c_6 \omega_p + c_7 t_s + c_8 \omega_s + c_9 (if\ \omega_p < \omega_{t_w}) \quad (8)$$

where, different types of number of heat transfer units (NTU) and dimensionless height (x*) are defined as: $NTU_p = \frac{h_p A}{m_p c_{pa}}$, $NTU_{mp} = \frac{h_{mp} A}{m_p}$, $NTU_s = \frac{h_s A}{m_s c_{pa}}$, $NTU_{ms} = \frac{h_{ms} A}{m_s}$, $NTU_e = Ah_{ms}$, $NTU_c = Ah_{mp}$, $x^* = \frac{x}{H}$. The heat transfer area (A) is calculated as: $A = 2n_p \cdot H \cdot L$ and the coefficients in the equations are defined as (a and b are constant, a=0.0012, b=-0.0107):

$$c_1 = \frac{h_p}{h_s + h_p + \sigma a h_{ms}(h_{fg} - c_{pw} t_{ew})}, c_2 = \frac{(h_{fg} - c_{pw} t_{ew}) h_{ms} \sigma}{h_s + h_p + \sigma a h_{ms}(h_{fg} - c_{pw} t_{ew})},$$

$$c_3 = \frac{h_s}{h_s + h_p + \sigma a h_{ms}(h_{fg} - c_{pw} t_{ew})}, c_4 = \frac{(c_{pw} t_{ew} - h_{fg}) h_{ms} b \sigma}{h_s + h_p + \sigma a h_{ms}(h_{fg} - c_{pw} t_{ew})},$$

$$c = h_s + h_p + a h_{fg}(\sigma h_{ms} + h_{mp}) - a c_{pw}(t_{ew} \sigma h_{ms} + t_{cw} h_{mp}), c_5 = \frac{h_p}{c}, c_6 = \frac{h_{fg} h_{mp} - c_{pw} t_{cw} h_{mp}}{c}, c_7 = \frac{h_s}{c},$$

$$c_8 = \frac{\sigma h_{fg} h_{ms} - \sigma c_{pw} t_{ew} h_{ms}}{c}, c_9 = \frac{b c_{pw}(t_{ew} h_{ms} \sigma + t_{cw} h_{mp}) - b h_{fg}(h_{ms} \sigma + h_{mp})}{c}.$$

The boundary conditions for the above governing equations are:

$$\begin{cases} x^* = 1, t_p = t_{p,in} \\ x^* = 1, \omega_p = \omega_{p,in} \\ x^* = 0, t_s = t_{s,in} \\ x^* = 0, \omega_s = \omega_{s,in} \\ x^* = 1, m_{cw} = 0 \\ x^* = 1, m_{ew} = m_{e,in} \end{cases}$$

The equation for calculating the heat transfer coefficient for the fully developed laminar flow in the parallel air channel is:

$$h_p = \frac{0.023\left(\frac{u_p}{\upsilon_p}\right)^{0.8} \cdot Pr_p^{0.3} \cdot \lambda_p}{d_e^{0.2}} \qquad (9)$$

where, d_e is the hydraulic diameter of the channel (m), calculated as $d_e=2s$.

The mass transfer coefficient (h_{mp}, h_{ms}) can be obtained accordingly by assuming Lewis relationship is satisfied and Lewis number is unity in air-water interaction surfaces [37~39]. So the mass transfer coefficient of primary air is:

$$h_{mp}=\frac{h_p}{c_{pa}Le_p^{2/3}}\approx\frac{h_p}{c_{pa}} \tag{10}$$

2.1.2 Power consumption

The energy consumption is another important aspect for evaluating the IEC performance. The energy consumption components of IEC include the supply air fan, exhaust air fan and circulation pump. The energy consumption of the pump is not discussed in the paper because it is very small and not related to the optimization process. The power of fans can be estimated by calculating the pressure drop using hydraulic calculation formulas:

$$\Delta P=\frac{f_{\mathrm{Re}}}{\mathrm{Re}}\cdot\frac{L}{d_e}\cdot\frac{\rho u^2}{2} \tag{11}$$

where, f_{Re} is the friction coefficient; *Re* is the Reynolds number, defined as $\mathrm{Re}=u\cdot d_e/\upsilon$.

The hydraulic diameter of the air channel is given by:

$$d_e=\frac{2ab}{a+b} \tag{12}$$

where, *a* and *b* are the long side and short side length of the cross section of the air channel, m.

The friction coefficient can be calculated by empirical formula:

$$f_{\mathrm{Re}} = 96(1 - 1.3553\alpha + 1.9467\alpha^2 - 1.7012\alpha^3 + 0.9564\alpha^4 - 0.2537\alpha^5) \quad (13)$$

where, α is the dimensionless shape factor, given by $\alpha=b/a$.

According to the experimental study, the resistance in the secondary air channel is 2.5~3 times larger than the fresh air channel owing to the interaction between the spraying water drops and air flow [40]. So the actual pressure drop in the fresh air channel and secondary air channel can be calculated separately as:

$$\Delta P_p = \Delta P \quad (14)$$

$$\Delta P_s = 3\Delta P \quad (15)$$

The power consumption of the primary fan is calculated as:

$$P_{p,fan} = \frac{Q \times \Delta P_p}{3600 \times 1000 \times \eta_0 \times \eta_1} \times K \quad (16)$$

where, $P_{\mathrm{p,fan}}$ is the power of the fan, kW; Q is the air flow rate, m^3/h; η_0 is the internal efficiency of the fan, ranging from 0.7~0.8; η_1 is the mechanical efficiency, ranging from 0.85~0.95; K is motor capacity coefficient, ranging from 1.05~1.1. In this study, the η_0, η_1 and K are supposed to be 0.75, 0.9 and 1.1, respectively. The power consumption of secondary air fan can be calculated similarly.

2.2 Model validation

An experimental test rig was built and measurement data was collected in order to validate the established model. The channel gap for the plate type IEC is 4mm with the unit geometry dimensions of 0.4m(L)×0.2m(W)×0.4m(H). The inlet and outlet temperature, relative humidity and air velocity of the primary air and secondary air were collected by the transmitters with the accuracy of ±0.3 ℃, ±2.5% RH and ±0.2m/s, respectively. A humidifier and an electric heater were installed inside the primary air duct with a PID controller to keep the air temperature at desired setting. Two fan speed controllers were used to adjust the flow rate of primary air and secondary air, respectively. By using these devices, the inlet primary air conditions can be adjusted to simulate the weather condition in both dry and humid regions. The exhausted air from an air-conditioned room with the temperature of 22℃~24℃ and relative humidity of 60% ~80% was used as secondary air.

The established model is validated under three operation conditions by the experiment data: non-condensation case with low primary air humidity, condensation case with high primary air humidity and dynamic transition from non-condensation to condensation. The overall experiment results of the former two operation states are presented in Fig.4. Fig.4 shows the comparison between simulation and experiment results of primary air temperature and moisture content drop between inlet and outlet. The temperature of the inlet primary air ranges from 27.1 ~ 34.4℃ and the moisture content ranges from 12.1 ~ 20.5 g/kg. The condensation state takes place when the inlet moisture content exceeds 15.5 g/kg according to the test results. It shows that the discrepancies between the experimental and simulated temperature drop ($(\Delta t_{p,exp} - \Delta t_{p,sim})/\Delta t_{p,exp} \times 100\%$) are within ±10% under both condensation and non-condensation states for majority

cases. The discrepancies between the experimental and simulated moisture content drop are found to be larger because of relatively small $\Delta\omega_p$ values and limitation of transmitters' accuracy. However, discrepancies of moisture content drop between experiment and simulation (($\Delta\omega_{p,exp}$ - $\Delta\omega_{p,sim}$)/$\Delta\omega_{p,exp}$ ×100%) are still within ±20% for majority cases.

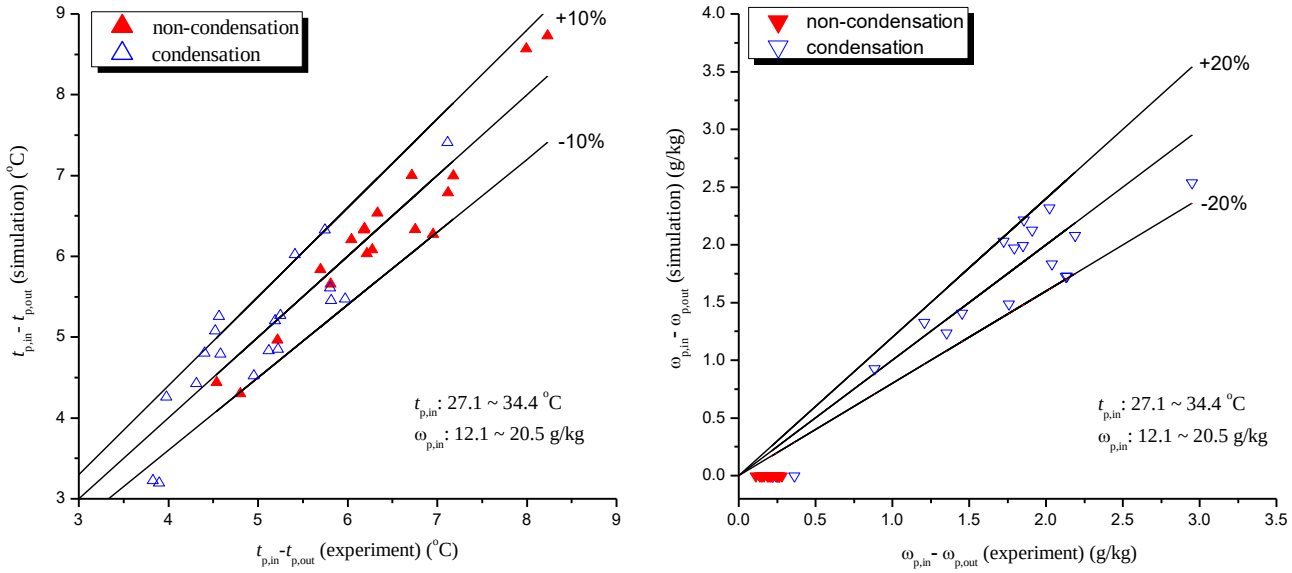

Fig.4 Comparison of temperature and moisture content drop between experiment and simulation

The influence of four controllable parameters (t_p, u_p, t_s, u_s) is also compared between simulation and experiment results. The results are given in wet-bulb efficiency ($\eta_{wb} = \frac{t_{p,in} - t_{p,out}}{t_{p,in} - t_{wb,s}}$) and latent efficiency ($\eta_{lat} = \frac{\omega_{p,in} - \omega_{p,out}}{\omega_{p,in} - \omega_{s,in}}$) as indicators, as shown in Fig.5. It can be seen that the model can well predict η_{wb} and η_{lat} in varying inlet conditions.

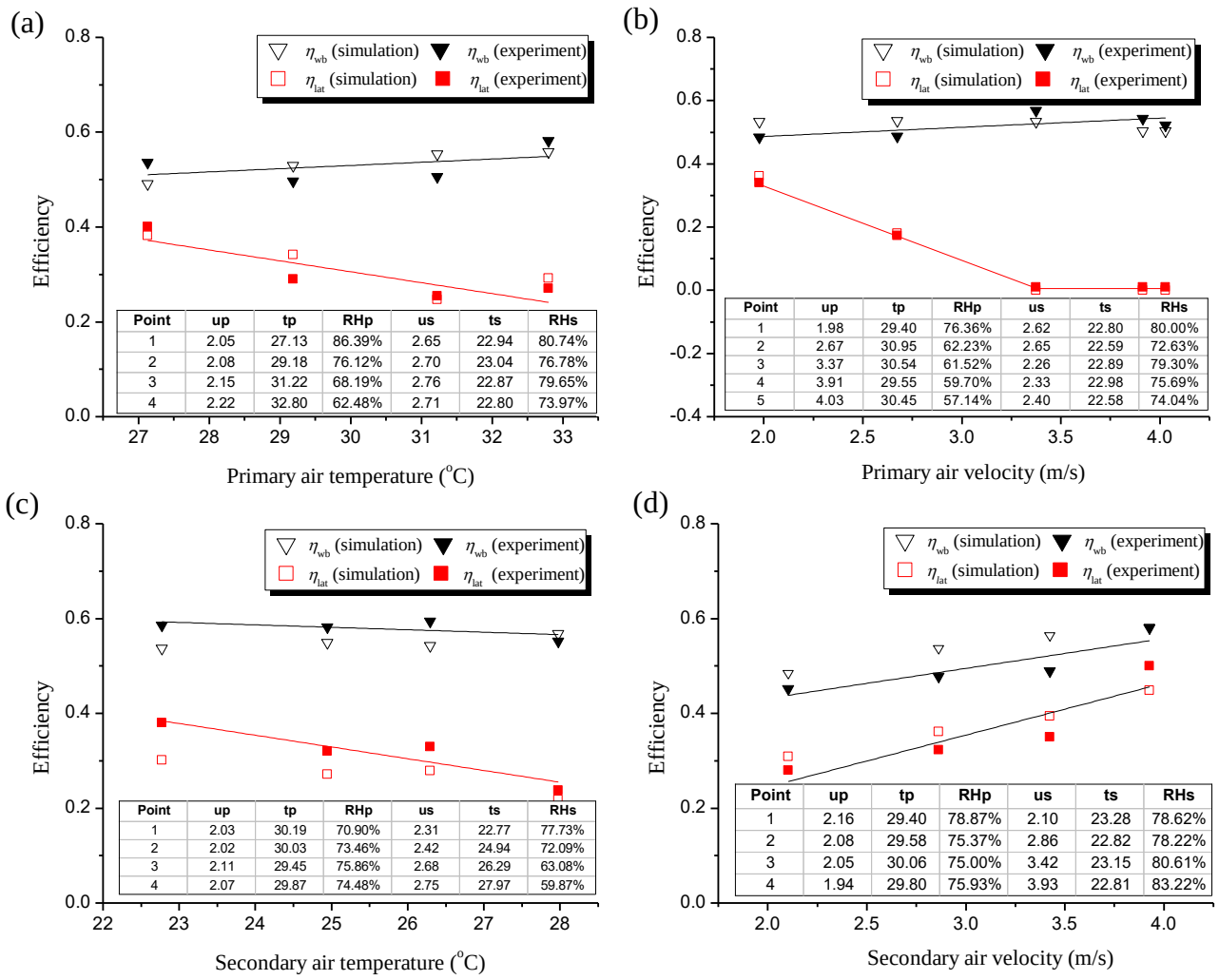

Fig.5 Influence of parameters compared between simulation and experiment: (a) influence of t_p; (b) influence of u_p; (c) influence of t_s; (d) influence of u_s

Fig.6 shows the transition of primary air outlet conditions from non-condensation to condensation state. The humidifier is turned off under non-condensation state and turned on under condensation state. It can be seen that the primary air outlet temperature keeps increasing and then remains steady at 24.7℃ after the humidifier turned on. The RH of inlet primary air increased from 48.8% to 84.7% after being humidified, changing the operation state from non-

condensation to condensation. The rise of outlet temperature is because the heat released during condensation process. Besides, the outlet moisture content decreases owing to the condensation or dehumidification. The simulation results of the final outlet temperature and humidity are marked in Fig.6. Good agreement can be found between the simulation and experiment results with the discrepancies of 1.8% for $t_{p,out}$ and 3.3% for $\omega_{p,out}$.

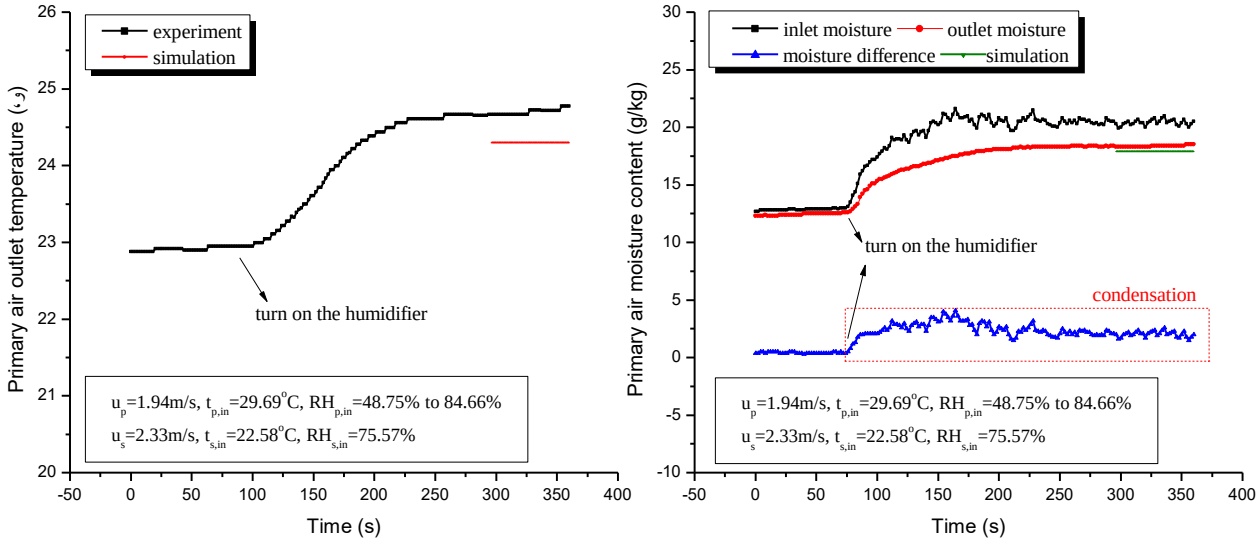

Fig.6 Transition of primary air outlet conditions from non-condensation to condensation

Based upon the experimental validation, the IEC model can be regarded as reliable for the following parameter sensitivity analysis and configuration optimization.

2.3 Evaluation index for IEC performance

The wet-bulb efficiency is usually used as an evaluation index for rating an IEC, which is expressed as [41]:

$$\eta_{wb} = \frac{t_{p,in} - t_{p,out}}{t_{p,in} - t_{wb,s}} \tag{17}$$

The wet-bulb efficiency describes the ability of IEC in handling sensible heat. Under the condensation state of IEC, other evaluation indexes are needed for evaluating the ability in handling the latent heat. Therefore, enlargement coefficient ε is introduced for evaluating the enlarged heat transfer rate associated with condensation, which is expressed as Eq.(18). The larger the ε, the more latent heat accounts for.

$$\varepsilon = \frac{Q_{tot}}{Q_{sen}} = \frac{c_{pa} \cdot m_p \cdot (t_{p,in} - t_{p,out}) + h_{fg} \cdot m_p \cdot (\omega_{p,in} - \omega_{p,out})}{c_{pa} \cdot m_p \cdot (t_{p,in} - t_{p,out})} \quad (18)$$

The total heat transfer rate can be calculated and rewritten as:

$$Q_{tot} = \varepsilon \cdot Q_{sen} = \varepsilon \cdot m_p \cdot c_{pa} \cdot (t_{p,in} - t_{p,out}) = \eta_{wb} \cdot \varepsilon \cdot m_p \cdot c_{pa} \cdot (t_{p,in} - t_{wb,s,in}) \quad (19)$$

The values of m_p, $t_{p,in}$ and $t_{wb,s,in}$ are decided by the air flow rate demand, outdoor weather condition and indoor design parameter. They are engineering uncontrollable once the application field selected. So, for a certain project, the value of $\eta_{wb} \cdot \varepsilon$ plays an important role in determining the total heat transfer rate and needs to be optimized. The synthetic index calculated by $\eta_{wb} \cdot \varepsilon$ is therefore proposed as the objective for optimization.

3. Sensitivity analysis

3.1 Orthogonal test

The orthogonal test is a high efficient, fast and economical design method for the multiple factors with multiple levels. By arranging the representative experiment reasonably using the orthogonal test table, the importance of each factor and optimized level combination can be obtained with minimal number of experiments.

Seven parameters (t_p, RH_p, t_s, RH_s, u_p/ u_s, s and H) are selected for the sensitivity analysis to determine the most influential parameters for IEC performance under condensation state. The rank of parameter influence on three indexes (wet-bulb efficiency η_{wb},, enlargement coefficient ε and synthetic index $\eta_{wb}\cdot\varepsilon$) are analysed. The rank of influence on η_{wb},, ε and $\eta_{wb}\cdot\varepsilon$ represent the rank of influence on sensible heat transfer, latent heat transfer and total heat transfer, respectively.

The ranges of t_p and RH_p are selected according to the weather condition in hot and humid regions; t_s and RH_s are based on the usual range in an air-conditioned room. In majority application cases, supply air to exhausted air rate ratio (u_p/u_s) equals to 1. However, in some special application fields, such as clean room and rooms contain contaminants, positive and negative pressure should be provided respectively to prevent contaminants entering or spreading outside the room. Therefore, u_p/u_s can be smaller or larger than 1. Besides, as the commonly recommended air velocity of IEC is 2~4 m/s considering the pressure drop and adequate heat transfer, u_p/u_s can range from 0.5 to 2. Based on the two points, the range of u_p/u_s is determined to be 0.5 ~2 in the sensitivity analysis. The u_s and L are set to be 2.0m/s and 0.5m, respectively. The number for channel pairs is 50 in the simulation. Three levels are selected for each parameter before the orthogonal test table can be determined. The ranges and levels of the parameters are listed in Table 1. The standard seven-parameter and three-level orthogonal test table $L_{18}(3^7)$ is selected and the simulation is conducted according to the arrangement of $L_{18}(3^7)$. The total number of simulation is 18 times, which is much less than the comprehensive simulation scheme (3^7=2187).

Table 1 Ranges and levels of the parameters in orthogonal test

No.	Parameter	Range	Level 1	Level 2	Level 3
1	t_p (℃)	30~38	30	34	38
2	RH_p (%)	60~90	60	75	90
3	t_s (℃)	22~28	22	25	28
4	RH_s (%)	40~70	40	55	70
5	u_p/ u_s	0.5~2	0.5	1.25	2
6	s (mm)	2~10	2	6	10
7	H (m)	0.5~2	0.5	1.25	2

3.2 Data analysis methods

Two methods were adopted in analysing the results of orthogonal test, called range method and analysis of variance method, respectively.

3.2.1 Range method

The range method is one of the most commonly used analysis methods. It can rank the influence of parameters and select the optimal combination of levels with simple calculation. However, it can not estimate the error and the accuracy is also limited. The influence of parameter can be evaluated by R_j in the range method, which is calculated as Eq.(20). The larger the R_j, the more influential the parameter.

$$R_j = \max[\bar{y}_{j1}, \bar{y}_{j2}, ...] - \min[\bar{y}_{j1}, \bar{y}_{j2}, ...] \quad (20)$$

where, R_j is the range of factor j; $\bar{y}_{jk}$ is the average of y_{jk}; y_{jk} is the sum of experimental index on level k of factor j.

Based on the range method, the parameter - index trend is usually used as a visualized way for displaying the influence of each parameter on the index. The level of the parameter is used as x-axis and the average index under different level is used as y-axis.

3.2.2 Analysis of variance method

Analysis of variance method is a rigorous statistical method for analyzing the data. It can provide accurate results on the ranking of parameter influence and significance test, but needs more complex calculation. The influence of parameter can be evaluated by total sum of squared deviations (*S*), calculated by Eq.(21). The larger the *S*, the more influential the parameter. The significant of a certain parameter can be investigated by F-test method.

The total sum of squared deviations is calculated as:

$$S = \sum_{i=1}^{a} (y_i - \bar{y})^2 = \sum_{i=1}^{a} y_i^2 - \frac{1}{a} (\sum_{i=1}^{a} y_i)^2 \qquad (21)$$

where, y_i is the experiment data at the time *i*; *a* is the number of experiment; $\bar{y}$ is the average value of the experiment data;

The sum of squared deviations in column *j* can be calculated as:

$$S_j = \frac{a}{b} \sum_{k=1}^{b} (\bar{y}_{jk} - \bar{y})^2 = \frac{b}{a} \sum_{k=1}^{b} y_{jk}^2 - \frac{1}{a} (\sum_{i=1}^{a} y_i)^2 \qquad (22)$$

where, *b* is the number of factor levels; $\bar{y}_{jk}$ is the average value for level *k* in column *j*;

The freedom of the total sum of squared deviations is:

$$f = a - 1 \tag{23}$$

The freedom of the sum of squared deviations in column j is:

$$f_j = b - 1 \tag{24}$$

The statistics index F_A is calculated as:

$$F_A = \frac{S_A / f_A}{S_e / f_e} \tag{25}$$

where, F_A is the F ratio of factor A; S_A is the sum of squared deviations of factor A; S_e is the sum of squared deviations of experimental error; f_A is the freedom of factor A and f_e is the freedom of error.

The threshold $F_{0.01}(f_A, f_e)(\alpha=0.01)$ for the freedom of f_A and freedom of f_e can be checked in the statistics toolbox. If $F_A > F_{0.01}(f_A, f_e)$, the influence of factor in column j is significate. If not, the influence is not significant.

The contribution ratio of factor j can be calculated as:

$$\rho_j = \frac{S_j - f_j \cdot V_e^{'}}{S}(\%) \tag{26}$$

where, $V_e^{'}$ is the average sum of squared deviations of errors.

4. Results and discussion

The results of parameter sensitivity analysis using range method and analysis of variance method are presented. The rank of parameter influence on η_{wb}, ε and $\eta_{wb}\cdot\varepsilon$ are presented as well as their contribution ratio and significance of influence. Then, the most influential and controllable parameters are selected for optimization.

4.1 Sensitivity analysis results

The orthogonal table $L_{18}(3^7)$ and corresponding simulation results are presented in Table 2. It can be seen from Table 2 that both η_{wb} and ε varies in a large range between 0.171 to 0.905 and 1.0 to 5.19, respectively, results in a variation of $\eta_{wb}\cdot\varepsilon$ from 0.49 to 3.39. Besides, a larger η_{wb} corresponds with a smaller ε. It means that under condensation condition, the latent heat transfer increases with the sensible heat transfer decreases. The index range of each parameter is calculated by the range method introduced in Section 3.2.1. In order to display the influence of each parameter in a visualized way, the factors - index trends are presented in Fig.7. In term of wet-bulb efficiency, the rank of influence for the seven parameters is $s > H > u_p/u_s > RH_p > RH_s > t_s > t_p$; for the enlargement coefficient is: $RH_p > t_p > u_p/u_s > RH_s > t_s > H > s$; for the synthetic index is: $s > H > u_p/u_s > RH_p > t_s > t_p > RH_s$. As the wet-bulb efficiency, enlargement coefficient and synthetic index reflect the effect of sensible heat transfer, latent heat transfer and total heat transfer, receptively, the rank of parameter influence on the three kind of heat transfer can be obtained.

Table 2 Simulation results of orthogonal test

Case	t_p (℃)	RH_p (%)	t_s (℃)	RH_s (%)	u_p/u_s	s (mm)	H (m)	η_{wb}	ε	$\eta_{wb}\cdot\varepsilon$
1	30	0.6	22	0.4	0.5	2	0.5	0.792	2.17	1.72
2	30	0.75	25	0.55	1.25	6	1.25	0.588	2.19	1.29
3	30	0.9	28	0.7	2	10	2	0.382	3.07	1.17
4	34	0.6	22	0.55	1.25	10	2	0.592	1.86	1.10
5	34	0.75	25	0.7	2	2	0.5	0.533	2.37	1.26
6	34	0.9	28	0.4	0.5	6	1.25	0.393	4.27	1.68
7	38	0.6	25	0.4	2	6	2	0.560	2.07	1.16
8	38	0.75	28	0.55	0.5	10	0.5	0.349	3.37	1.18
9	38	0.9	22	0.7	1.25	2	1.25	0.692	4.71	3.26
10	30	0.6	28	0.7	1.25	6	0.5	0.491	1.00	0.49
11	30	0.75	22	0.4	2	10	1.25	0.331	2.22	0.74
12	30	0.9	25	0.55	0.5	2	2	0.905	3.74	3.39
13	34	0.6	25	0.7	0.5	10	1.25	0.682	1.68	1.14
14	34	0.75	28	0.4	1.25	2	2	0.773	3.02	2.34
15	34	0.9	22	0.55	2	6	0.5	0.209	4.28	0.89
16	38	0.6	28	0.55	2	2	1.25	0.663	1.85	1.23
17	38	0.75	22	0.7	0.5	6	2	0.860	3.58	3.08
18	38	0.9	25	0.4	1.25	10	0.5	0.171	5.19	0.89

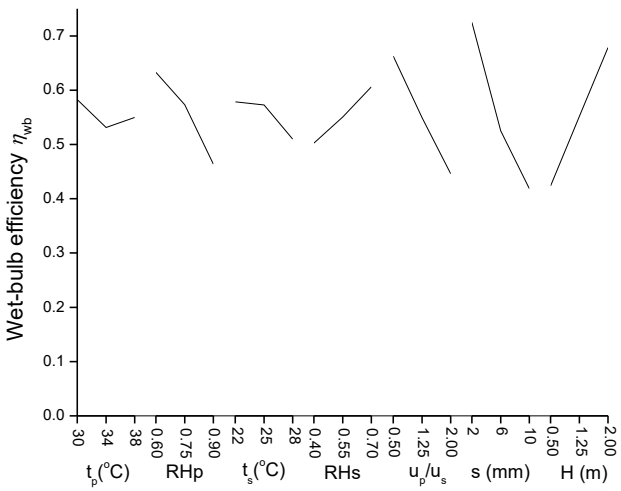

(a) Factors - η_{wb} trend

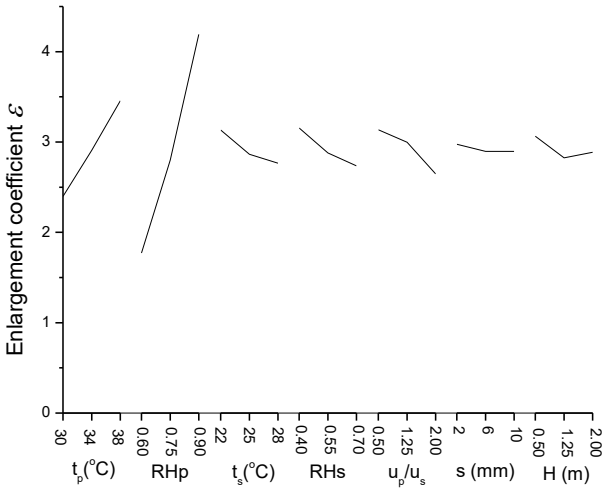

(b) Factor - ε trend

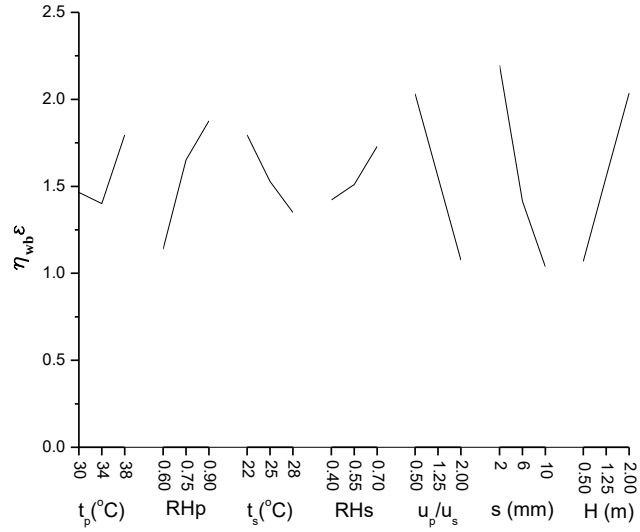

(c) Factor - $\varepsilon \cdot \eta_{wb}$ trend

Fig.7 Factors - index trend calculated by range method

The analysis of variance method can provide more accurate results and more information (Table 3) compared with the range method. In addition, the F-test can be used for judging the significance of a parameter. The parameter which has a significant impact on the index is marked with '√' in Table 3. It can be seen from Table 3, the rank of parameter influence is the same with

what obtained from the range method. For the wet-bulb efficiency, the rank is: $s > H > u_p/u_s > RH_p > RH_s > t_s > t_p$; for the enlargement coefficient is: $RH_p > t_p > u_p/u_s > RH_s > t_s > H > s$; for the synthetic index is: $s > H > u_p/u_s > RH_p > t_s > t_p > RH_s$.

Table 3 Results by analysis of variance method

Parameter / Index	t_p (℃)	RH_p (%)	t_s (℃)	RH_s (%)	u_p/u_s	s (mm)	H (m)
Variance analysis results for η_{wb}							
Variance	0.008	0.091	0.019	0.032	0.142	0.298	0.195
Contribution ratio	7.1%	10.6%	1.4%	3.1%	17.0%	37.0%	23.8%
Significance*						√	√
Variance analysis results for ε							
Variance	3.398	17.974	0.443	0.553	0.766	0.026	0.190
Contribution ratio	14.4%	76.9%	1.8%	2.3%	3.2%	0.8%	0.7%
Significance*	√	√		√	√		
Variance analysis results for $\eta_{wb} \cdot \varepsilon$							
Variance	0.544	1.711	0.625	0.314	2.731	4.203	2.801
Contribution ratio	1.8%	10.8%	2.4%	17.0%	18.7%	30.1%	19.2%
Significance**						√	√

* α=0.05 was used for F-test.

** α=0.1 was used for F-test.

From Table 3, we can see that the wet-bulb efficiency is greatly influenced by the channel gap and cooler height, while the enlargement coefficient is mainly decided by the primary air humidity, which contributes 76.9% to the influence. Channel gap and cooler height have significant influence on the synthetic index, which contribute 30.1% and 19.2%, receptively. Because the synthetic index reflects the total heat transfer process in the IEC operation, which is the most important concern in its design and operation, the channel gap and cooler height are selected as the most influential and engineering controllable parameters to be optimized in the next section.

4.2 Optimization of key parameters

The channel gap and cooler height are two controllable parameters in the design process and they have great influence on the IEC performance according to the sensitivity analysis, therefore their values needs to be optimized based on reasonable ranges of other parameters that are outside of engineering control. As the cooler height varies with the shape of the IEC, it is hard to be used as an index for the optimization. So the optimized results can be given in NTU values for universal reference for the two reasons: 1. cooler height is the only factor affects the heat transfer area ($A=H\cdot L\cdot 2n_p$) as the cooler length and channel pairs are fixed in the study; 2. heat transfer area is the only factor influences the NTU if the channel gap and inlet air conditions are fixed.

4.2.1 Parameter setting

The parameter values in IEC optimization are listed in Table 4. The channel gap varied from 2mm to 10mm when optimized while the other parameters kept unchanged at certain levels. As the optimized channel gap obtained from this paper is within the range of 2~5mm, and 2~5mm gap is also the normal dimension for the market products, the cooler height is therefore

optimized under the two limits of channel gap. The cooler height varies from 0.2~1.2m under s=2mm and 0.5~3.0m under s=5mm when optimized in order to restrict NTU within a normal range. Two representative levels of primary air temperature (30℃, 35℃) and three relative humidity (40%, 60%, 80%) are selected to represent the weather condition in hot and dry regions, hot and mid-humid regions as well as hot and humid regions. In IEC pre-cooling system, t_s and RH_s generally vary within a relatively small range as the exhausted air from air-conditioned space is used. So a constant t_s and RH_s (24℃, 60%) are used in the optimization. The u_p/u_s is set to be 1 because the fresh air supply rate is usually equal to the air exhaust rate in order to keep a normal indoor pressure.

Table 4 Parameter values in IEC optimization

Parameter	Optimization parameter	
	s (mm)	H (m)
t_p	30℃, 35℃	30℃, 35℃
RH_p	40%, 60%, 80%	40%, 60%, 80%
t_s	24℃	24℃
RH_s	60%	60%
u_p/ u_s	1	1
s	2~10mm	2mm, 5mm
H	0.5m, 1.0m	0.2~1.2m (s=2mm, NTU_p: 1.7~10.3) 0.5~3.0m (s=5mm, NTU_p: 1.4~8.5)

4.2.2 Optimization of channel gap

According to previous research, the smaller the channel gap, the higher the IEC efficiency. However, the smaller channel gap can lead to larger pressure loss so that the energy consumption by the fan would increase. So there should be a trade-off between the efficiency improvement and energy consumption. In this study, a net energy saving is proposed as an optimization objective, which is given by:

$$E_{net} = E_{saving} - E_{fan} \tag{27}$$

$$E_{saving} = \frac{Q_{saving}}{COP} = \frac{m_p \cdot (i_{p,in} - i_{p,out})}{COP} \tag{28}$$

where, E_{net} is the net energy saving by IEC, W; E_{saving} is the total energy saving by IEC, W; E_{fan} is the energy consumption by the primary and secondary air fans, W; Q_{saving} is the total heat recovery by IEC, W; COP is the coefficient of performance of a central air-conditioning unit, which is set to be 4.5 in the study.

The model introduced in Section 2.1.2 was adopted to calculate the fan consumption. Fig.8 presents the fan consumption under different channel gap. It can be seen that the fan consumption decreases as the channel gap increases and it drops dramatically when the channel gap increases from 2mm to 4mm.

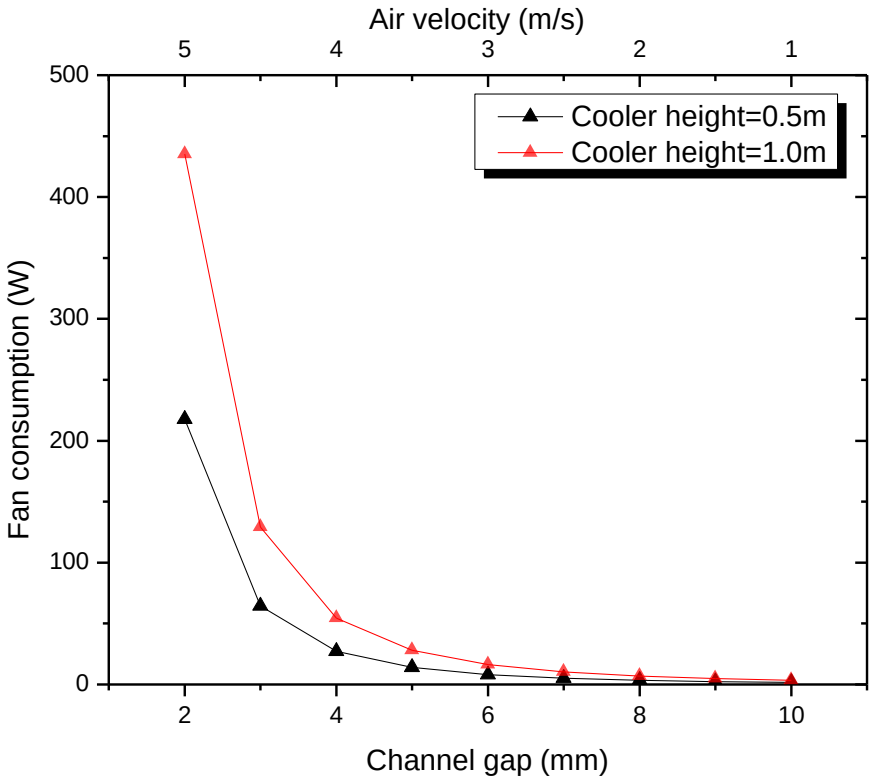

Fig.8 Fan consumption under different channel gap

Fig.9 shows the total energy saving by IEC under different channel gap, which is calculated as: $E_{saving}=m_p\cdot(i_{p,in}-i_{p,out})/COP$. It can be seen that the saving decreases with the increase of channel gap, especially within the channel gap between 2mm to 4mm. It is because the larger the channel gap, the more air is by-passed directly without heat transfer with the cold surface. Besides, it can be noticed that the energy saving of IEC under condensation state is larger than that of non-condensation state. It can be attributed to the condensation enlarges the total heat transfer rate by bringing in latent heat transfer. In addition, the decrease trend of the total energy saving under condensation is more significant than that of non-condensation state, especially when the channel gap ranges from 2mm to 4mm.

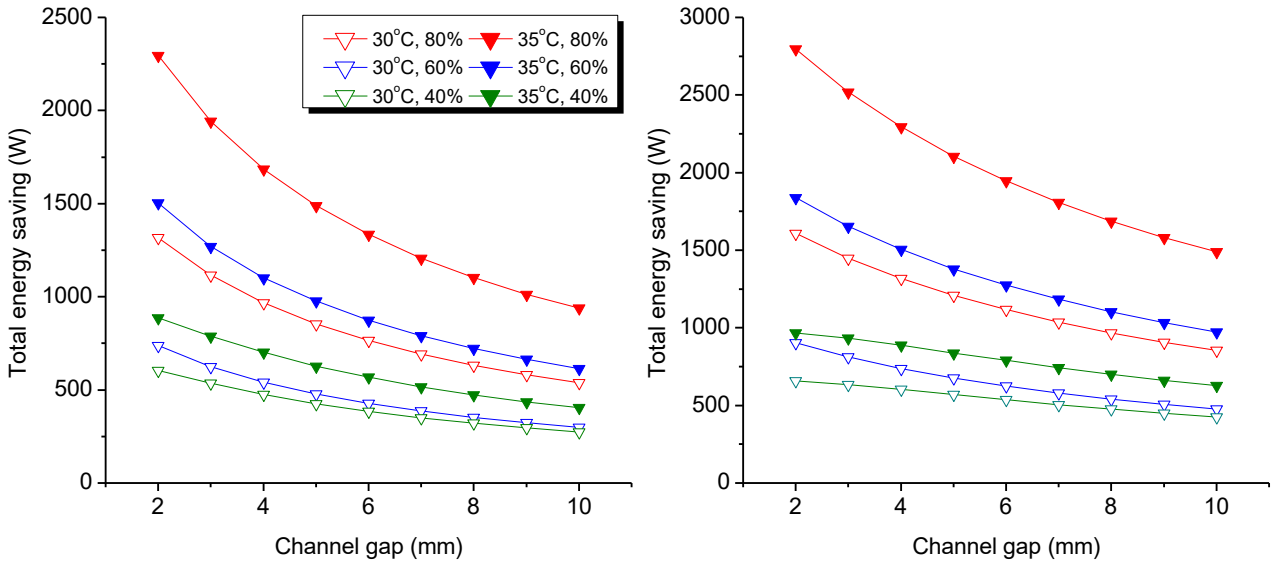

(a) Cooler height=0.5m (b) Cooler height=1.0m

Fig.9 Total energy saving under different channel gap

Fig.10 presents the net energy saving under different channel gap. The optimal channel gap is achieved when the net energy saving is the largest. The net energy saving reaches the peak point when the channel gap ranges from 3mm to 4mm under the dry primary air condition (RH=40%); while it ranges from 2mm to 3mm under the humid primary air condition (RH=60% and 80%). So the optimal channel gap of IEC under condensation state is a little smaller than that of traditional non-condensation state. It can be explained as follows. The total energy saving under condensation state increases more rapidly with the decrease of channel gap because of simultaneous enhancement of sensible and latent heat transfer processes. The consumption of the fans, however, remains almost unchanged.

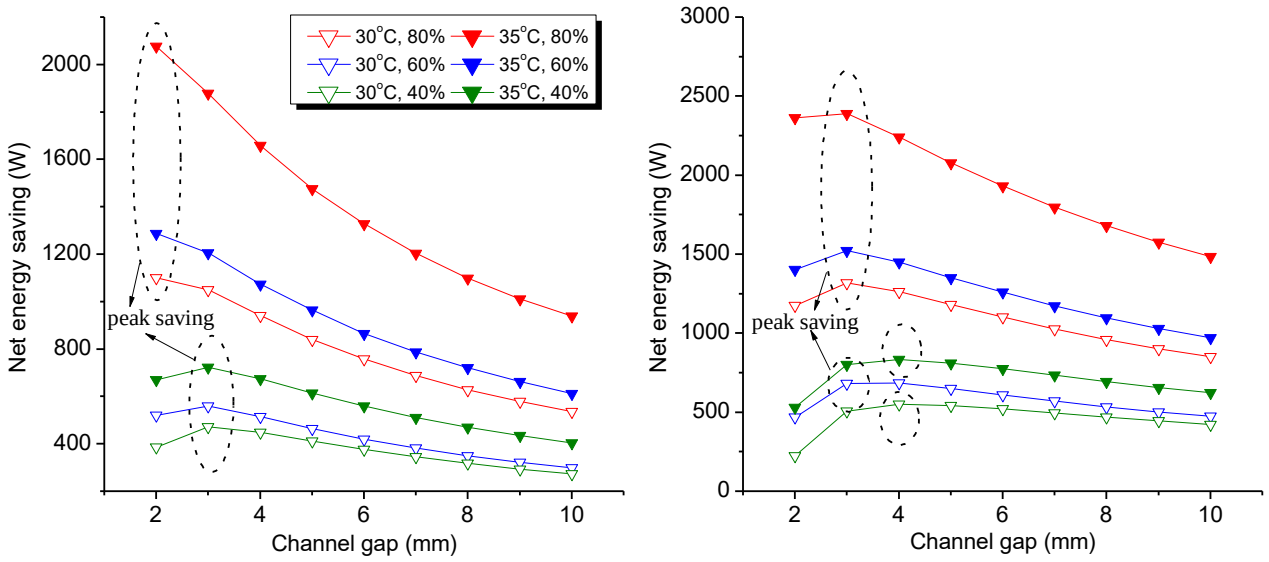

(a) Cooler height=0.5m (b) Cooler height=1.0m

Fig.10 Net energy saving under different channel gap

4.2.3 Optimization of cooler height

The increase of cooler height, on one hand, improves the efficiency by adding the heat transfer area, but on the other hand, increases the pressure drop of IEC and its manufacturing cost. So there is a trade-off between the improvement of efficiency and increase of fan consumption and equipment manufacturing cost. Similarly, net money saving is proposed as an optimization objective which is calculated as:

$$M_{net} = E_{pri} \cdot (E_{saving} - E_{fan}) - \frac{I}{365 \times 24 \times T} \qquad (29)$$

where, M_{net} is the net money saving of IEC, HKD/h; E_{pri} is the electricity price, HKD/kWh; I is the initial investment of IEC, HKD; T is the lifetime of IEC, which is set as 10 years.

The manufacturing cost of IEC is assumed to be in direct proportion to its heat transfer area.

$$I = A \cdot C_{IEC} = 2 \cdot H \cdot L \cdot n_p \cdot C_{IEC} \qquad (30)$$

where, C_{IEC} is the manufacturing cost per unit area, HKD/m^2, which is set to be 150 HKD/m^2 based on the average quotation on the market.

Fig.11 shows the fan consumption under different cooler height. Because the cooler height can not be easily used as an index for IEC with different shape, $NTU_p=(h_p \cdot A)/(m_p c_{pa})$ is used as the optimization index in this research as stated previously. We can see that the fan consumption increases linearly with the increase of cooler height and NTU_p.

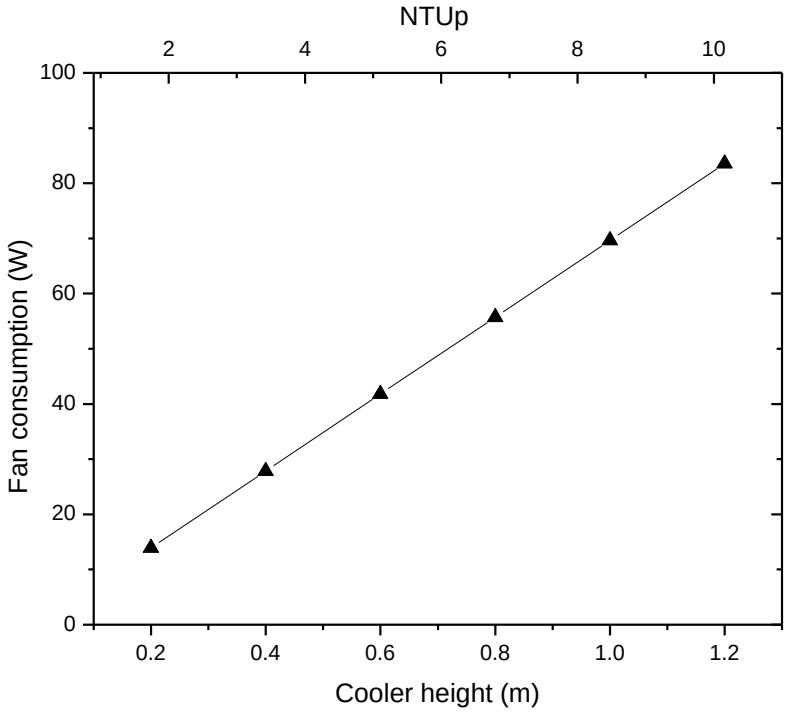

Fig.11 Fan consumption under different cooler height

The total energy saving under different cooler height and NTU_p is presented in Fig.12. The total energy saving increases with the increase of NTU_p, but the increase rate slows down when NTU_p reaches a certain value. It was found the slow-down trend under condensation state is less

obvious than that of non-condensation state. It can be seen from Fig.12 that the total energy saving under the low primary air humidity (RH=40%) remains almost steady when NTU_p exceeds 4.0. However, it keeps increasing until NTU_p exceeds 8.0 under high humidity air condition.

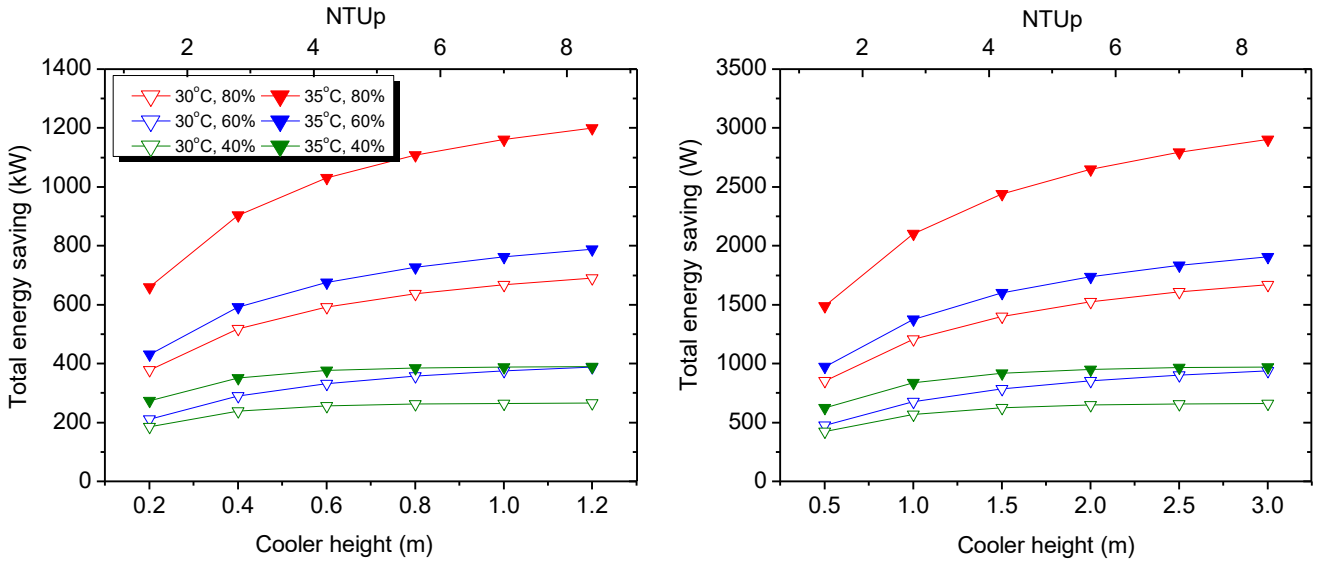

(a) Channel gap s=2mm

(b) Channel gap s=5mm

Fig.12 Total energy saving under different cooler height

Fig.13 presents the net money saving under different cooler height and NTU_p. The peak net saving is achieved when NTU_p is about 3~4 under low primary air humidity, while it remains almost steady when NTU_p reaches 5~7 under high primary air humidity. It means that the heat transfer area of IEC should be manufactured larger when applied in humid regions. It can be explained as follows. Under the condensation operation of IEC, the larger heat transfer area not only improves the sensible heat transfer rate but also increases the latent heat transfer rate. The benefit brought by the total energy saving increase is more than the additional consumption by the fan when adding the heat transfer area.

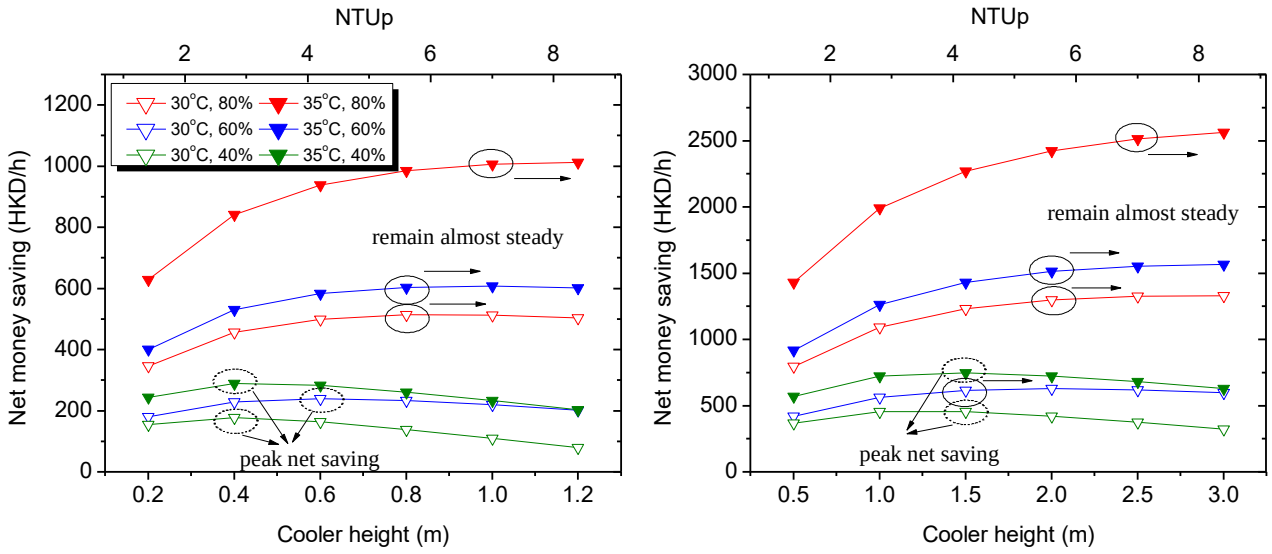

(a) Channel gap s=2mm (b) Channel gap s=5mm

Fig.13 Net money saving under different cooler height

As the manufacturing cost of IEC is a big unknown and varies greatly in different manufactories, three levels of manufacturing cost from 100 to 200 HKD/m^2 were selected to investigate the influence of manufacturing cost on the optimal NTU_p. The results are shown in Fig.14. It can be seen that the influence of manufacturing cost has a limited influence on the IEC optimal NTU_p, especially when the channel gap is very small. Under the channel gap of 2mm, the optimal NTU_p under IEC condensation state is about 5~7 when the manufacturing cost ranges from 100 HKD/m^2 to 200 HKD/m^2, which is larger than that of non-condensation state. Under the channel gap of 5mm, the situation can be slightly different. The optimal NTU_p increases a little as the manufacturing cost decreases from 200 HKD/m^2 to 100 HKD/m^2 on both non-condensation and condensation state. It means that the heat transfer area of IEC should be manufactured to be larger when the manufacturing cost is lower. Overall, the optimal NTU_p is about 3~4 (non-

condensation) and 4~7 (condensation) under 200 HKD/m^2 manufacturing cost, while it increases to about 4~5 (non-condensation) and 5~7 (condensation) under 100 HKD/m^2 manufacturing cost.

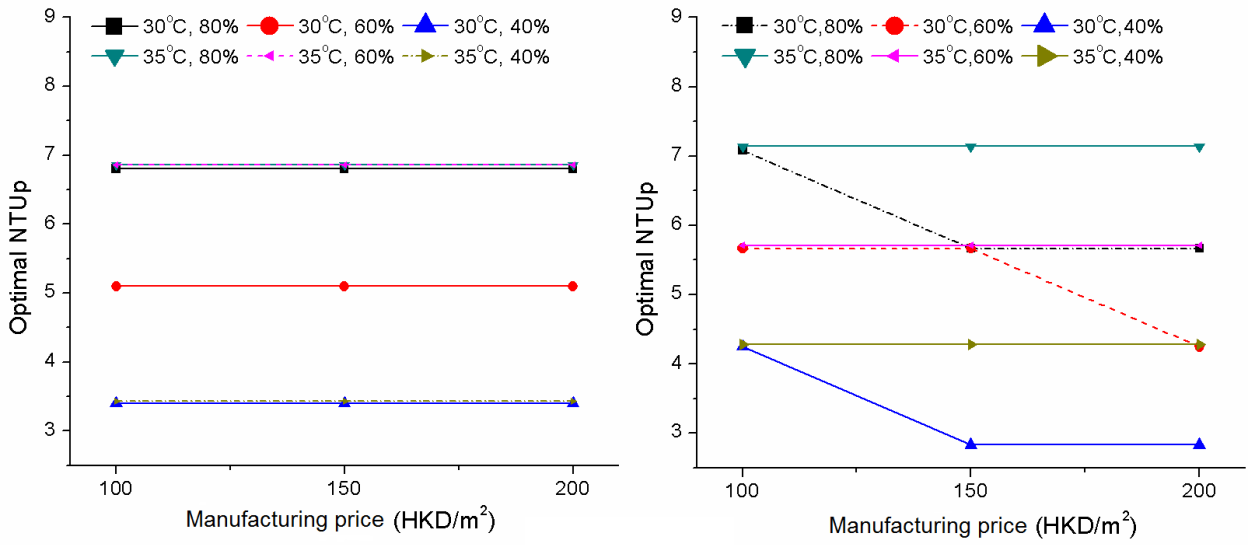

(a) channel gap s=2mm (b) channel gap s=5mm

Fig.14 Optimal NTU_p under different manufacturing price of IEC

The main benefit of IEC application in an air-conditioning system is energy saving, which can be converted into electricity bill saving in industry. Fig.15 presents the influence of electricity price on the optimal NTU_p of IEC. It can be seen that the optimal NTU_p decreases with the decrease of electricity price under both condensation and non-condensation states. It means that the IEC should be manufactured to be larger if the electricity price is high, so that more bill fee can be saved. Under the channel gap of 5mm, the optimal NTU_p is about 4~5 when the electricity price is 1.3 HKD/kWh and it drops to about 3~4 when electricity price decreases to 0.7 HKD/kWh under non-condensation state. Under condensation state, the optimal NTU_p is about 6~7 under the electricity price of 1.3 HKD/kWh and it drops to 4~6 when the electricity price is 0.7 HKD/kWh.

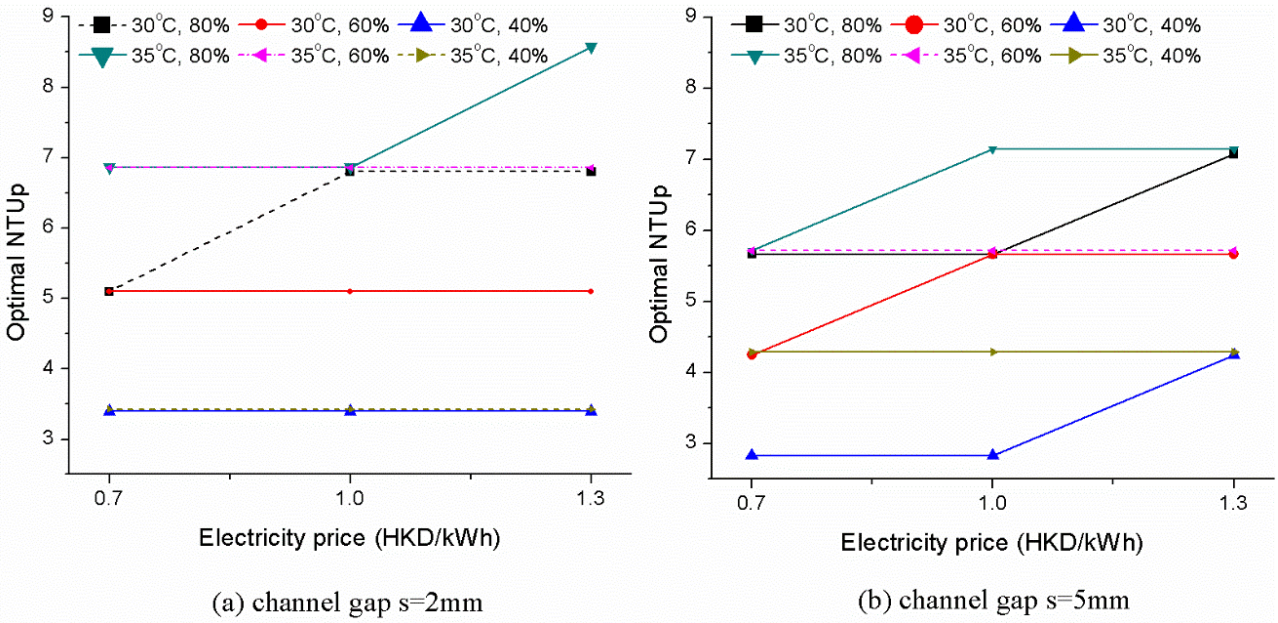

Fig.15 Optimal NTU_p under different electricity price

In sum, the optimal NTU_p of IEC in pre-cooling system is 3~5 under non-condensation state and 4~7 under condensation state by considering the thermal performance, fan consumption, manufacturing price and electricity price. The results compared with other relevant literatures are listed in Table 5.

Table 5 Results comparison with other literatures

Ref.	IEC type and flow pattern	Optimized parameter	Application
[32]	Combined parallel and counter flow	NTU_p:1.5~2.8	Cooling alone
[26]	Traditional and regenerative, cross flow	NTU_p≈5.0	Cooling alone
[30]	Traditional IEC, cross flow	NTU_p≈6.0	summer: IEC winter: HE
	Unidirectional flow	NTU_p=4;	

[29]	Counter flow Two closed loop with extraction	NTU_p=7; NTU_p=10	Cooling alone
[42]	regenerative IEC	*s*: 4~6 mm	Cooling alone
[23]	M-cycle cross-flow IEC	*s*: ≤4 mm	Cooling alone
Present	Traditional, counter flow	NTU_p: 3~5; *s*: 3~4 mm (non-con) NTU_p: 4~7; *s*: 2~3 mm (condensation)	Pre-cooling

5. Conclusion

The parameter sensitivity analysis was conducted on the indirect evaporative cooler (IEC) using the established model considering condensation. The sensitivity of seven parameters (t_p, RH_p, t_s, RH_s, u_p/u_s, *s*, *H*) on three evaluation indexes (η_{wb}, ε, $\eta_{wb}\cdot\varepsilon$) were analyzed in order to rank their influence under IEC condensation state. At last, configuration optimization was conducted to the most influential and engineering controllable parameters. The main research results were summarized as follows:

1) A numerical model of IEC considering condensation from primary air was established and validated by the experiment data. It was found that the discrepancy between the experimental and simulated temperature drop ($(\Delta t_{p,exp} - \Delta t_{p,sim})/\Delta t_{p,exp} \times 100\%$) is within ±10%; and the discrepancy between the experimental and simulated moisture content drop ($(\Delta \omega_{p,exp} - \Delta \omega_{p,sim})/\Delta \omega_{p,exp} \times 100\%$) is within ±20%.

2) Unlike the previous reported studies for IEC with no condensation, in current study, the sensitivity analysis of IEC under condensation condition was conducted and influence ranking of each parameter was reported. The sensitivity analysis was conducted among seven parameters (t_p, RH_p, t_s, RH_s, u_p/u_s, s, H) using orthogonal test. The enlargement coefficient and synthetic index were proposed to evaluate the latent and total heat transfer performance of condensation condition. The channel gap and cooler height were found to have significant impact on the wet-bulb efficiency η_{wb}; the primary air humidity had the dominate influence on the enlargement coefficient ε and the channel gap and cooler height had the most important effect on the synthetic index $\eta_{wb} \cdot \varepsilon$. The influence rank of parameters for the synthetic index is: $s > H > u_p/u_s > RH_p > t_s > t_p > RH_s$.
3) The optimized channel gap and NTU_p under IEC condensation condition in this study were found to be different from previous reported studies, in which condensation was not considered. The optimized channel gap of IEC is 2~3mm and NTU_p was 4~7 under condensation state; while it is 3~4mm and 3~5 under non-condensation state. Thus, in practical engineering, the channel gap of IEC should be manufactured to be a little smaller and heat transfer area should be manufactured to be larger than that of dry regions when IEC used in humid area where condensation may likely take place. Besides, the heat transfer area of IEC should be made larger when the manufacturing cost is lower and the electricity price is higher.

In sum, unlike the previous studies of IEC with no condensation, in current study, the sensitivity analysis and optimization of IEC under condensation condition was reported. The results reported in this paper are the first of their kinds in the open literature and can therefore, be used

as an important reference for the optimization of IEC design and operation in hot and humid regions, where IEC acts as a pre-cooling and heat recovery device in an air-conditioning system.

Acknowledgement

This research is financially supported by the Research Institute for Sustainable Urban Development (RISUD) of The Hong Kong Polytechnic University.

References

[1] Liu, Z., Allen, W., & Modera, M. (2013). Simplified thermal modeling of indirect evaporative heat exchangers. HVAC&R Research, 19(3), 257-267.

[2] Gómez, E. V., González, A. T., & Martínez, F. J. R. (2012). Experimental characterisation of an indirect evaporative cooling prototype in two operating modes. Applied Energy, 97, 340-346.

[3] Porumb, B., Ungureşan, P., Tutunaru, L. F., Şerban, A., & Bălan, M. (2016). A Review of Indirect Evaporative Cooling Operating Conditions and Performances. Energy Procedia, 85, 452-460.

[4] Maheshwari, G. P., Al-Ragom, F., & Suri, R. K. (2001). Energy-saving potential of an indirect evaporative cooler. Applied Energy, 69(1), 69-76.

[5] Chua, K. J., Chou, S. K., Yang, W. M., & Yan, J. (2013). Achieving better energy-efficient air conditioning–a review of technologies and strategies. Applied Energy, 104, 87-104.

[6] Porumb, B., Ungureşan, P., Tutunaru, L. F., Şerban, A., & Bălan, M. (2016). A Review of Indirect Evaporative Cooling Technology. Energy Procedia, 85, 461-471.

[7] Krüger, E., González Cruz, E., & Givoni, B. (2010). Effectiveness of indirect evaporative cooling and thermal mass in a hot arid climate. Building and Environment, 45(6), 1422-1433.

[8] Jaber, S., & Ajib, S. (2011). Evaporative cooling as an efficient system in Mediterranean region. Applied Thermal Engineering, 31(14), 2590-2596.

[9] Bajwa, M., Aksugur, E., & Al-Otaibi, G. (1993). The potential of the evaporative cooling techniques in the gulf region of the Kingdom of Saudi Arabia. Renewable energy, 3(1), 15-29.

[10] Chen PL, Qin H, Huang YJ, Wu H, Blumstein C. The energy-saving potential of precooling incoming outdoor air by indirect evaporative cooling. ASHRAE Trans 1993;99(Pt 1).

[11] Delfani, S., Esmaeelian, J., Pasdarshahri, H., & Karami, M. (2010). Energy saving potential of an indirect evaporative cooler as a pre-cooling unit for mechanical cooling systems in Iran. Energy and Buildings, 42(11), 2169-2176.

[12] Cianfrini, C., Corcione, M., Habib, E., & Quintino, A. (2014). Energy performance of air-conditioning systems using an indirect evaporative cooling combined with a cooling/reheating treatment. Energy and Buildings, 69, 490-497.

[13] Jain, V., Mullick, S. C., & Kandpal, T. C. (2013). A financial feasibility evaluation of using evaporative cooling with air-conditioning (in hybrid mode) in commercial buildings in India. Energy for Sustainable Development, 17(1), 47-53.

[14] Chen, Y., Luo, Y., & Yang, H. (2015). A simplified analytical model for indirect evaporative cooling considering condensation from fresh air: Development and application. Energy and Buildings, 108, 387-400.

[15] Chen, Y., Luo, Y., & Yang, H. (2014). Fresh air pre-cooling and energy recovery by using indirect evaporative cooling in hot and humid region–a case study in Hong Kong. Energy Procedia, 61, 126-130.

[16] Xuan, Y. M., Xiao, F., Niu, X. F., Huang, X., & Wang, S. W. (2012). Research and application of evaporative cooling in China: A review (I)–Research. Renewable and Sustainable Energy Reviews, 16(5), 3535-3546.

[17] Maisotsenko, V., Gillan, L. E., Heaton, T. L., & Gillan, A. D. (2003). U.S. Patent No. 6,581,402. Washington, DC: U.S. Patent and Trademark Office.

[18] Cui, X., Chua, K. J., & Yang, W. M. (2014). Numerical simulation of a novel energy-efficient dew-point evaporative air cooler. Applied Energy, 136, 979-988.

[19] Jradi, M., & Riffat, S. (2014). Experimental and numerical investigation of a dew-point cooling system for thermal comfort in buildings. Applied Energy, 132, 524-535.

[20] Hasan, A. (2012). Going below the wet-bulb temperature by indirect evaporative cooling: analysis using a modified ε-NTU method. Applied Energy, 89(1), 237-245.

[21] Hasan, A. (2010). Indirect evaporative cooling of air to a sub-wet bulb temperature. Applied Thermal Engineering, 30(16), 2460-2468.

[22] Guo, X. C., & Zhao, T. S. (1998). A parametric study of an indirect evaporative air cooler. International communications in heat and mass transfer, 25(2), 217-226.

[23] Zhan, C., Zhao, X., Smith, S., & Riffat, S. B. (2011). Numerical study of a M-cycle cross-flow heat exchanger for indirect evaporative cooling. Building and Environment, 46(3), 657-668.

[24] Lee, J., & Lee, D. Y. (2013). Experimental study of a counter flow regenerative evaporative cooler with finned channels. International Journal of Heat and Mass Transfer, 65, 173-179.

[25] Riangvilaikul, B., & Kumar, S. (2010). Numerical study of a novel dew point evaporative cooling system. Energy and Buildings, 42(11), 2241-2250.

[26] Bolotin, S., Vager, B., & Vasilijev, V. (2015). Comparative analysis of the cross-flow indirect evaporative air coolers. International Journal of Heat and Mass Transfer, 88, 224-235.

[27] Kim, M. H., Jeong, D. S., & Jeong, J. W. (2015). Practical thermal performance correlations for a wet-coil indirect evaporative cooler. Energy and Buildings, 96, 285-298.

[28] Yuan, F., & Chen, Q. (2012). A global optimization method for evaporative cooling systems based on the entransy theory. Energy, 42(1), 181-191.

[29] Hsu, S. T., Lavan, Z., & Worek, W. M. (1989). Optimization of wet-surface heat exchangers. Energy, 14(11), 757-770.

[30] Anisimov, S., Pandelidis, D., & Jedlikowski, A. (2015). Performance study of the indirect evaporative air cooler and heat recovery exchanger in air conditioning system during the summer and winter operation. Energy, 89, 205-225.

[31] Pandelidis, D., & Anisimov, S. (2015). Numerical analysis of the heat and mass transfer processes in selected M-Cycle heat exchangers for the dew point evaporative cooling. Energy Conversion and Management, 90, 62-83.

[32] Anisimov, S., Pandelidis, D., & Danielewicz, J. (2015). Numerical study and optimization of the combined indirect evaporative air cooler for air-conditioning systems. Energy, 80, 452-464.

[33] Goldsworthy, M., & White, S. (2011). Optimisation of a desiccant cooling system design with indirect evaporative cooler. International Journal of refrigeration, 34(1), 148-158.

[34] Cui, X., Chua, K. J., Islam, M. R., & Ng, K. C. (2015). Performance evaluation of an indirect pre-cooling evaporative heat exchanger operating in hot and humid climate. Energy Conversion and Management, 102, 140-150.

[35] Yang, H., Ren, C., & Cui, P. (2006). Study on performance correlations of an indirect evaporative cooler with condensation from primary airflow. HVAC&R Research, 12(3), 519-532.

[36] Chen, Y., Yang, H., & Luo, Y. (2016). Indirect evaporative cooler considering condensation from primary air: Model development and parameter analysis. Building and Environment, 95, 330-345.

[37] ASHRAE. Fundamentals, American Society of Heating, Refrigeration and Air Conditioning Engineers, USA; 1997.

[38] ASHRAE Handbook: Fundamentals. Mass transfer, Atlanta, GA; 2005. p. 9 (Ch.5).

[39] Huang, C. C., Yan, W. M., & Jang, J. H. (2005). Laminar mixed convection heat and mass transfer in vertical rectangular ducts with film evaporation and condensation. International journal of heat and mass transfer, 48(9), 1772-1784.

[40] Zhao Z, Ren C, Tu M, et al (2010) , Experimental investigation on plate type heat exchanger used as indirect evaporative cooler, Journal of refrigeration, 31(1), 45~49.

[41] Duan, Z., Zhan, C., Zhang, X., Mustafa, M., Zhao, X., Alimohammadisagvand, B., & Hasan, A. (2012). Indirect evaporative cooling: Past, present and future potentials. Renewable and Sustainable Energy Reviews, 16(9), 6823-6850.

[42] Fakhrabadi, F., & Kowsary, F. (2016). Optimal design of a regenerative heat and mass exchanger for indirect evaporative cooling. Applied Thermal Engineering, 102, 1384-1394.